Nano Energy 24 (2016) 72–77

Contents lists available at ScienceDirect

Nano Energy

journal homepage: www.elsevier.com/locate/nanoen

Flexible, three-dimensional ordered macroporous TiO_2 electrode with enhanced electrode–electrolyte interaction in high-power Li-ion batteries

Gregory Lui [a], Ge Li [a], Xiaolei Wang [a], Gaopeng Jiang [a], Edric Lin [a], Michael Fowler [a], Aiping Yu [a,*], Zhongwei Chen [a,*]

[a] Department of Chemical Engineering, University of Waterloo, 200 University Avenue West, Waterloo, ON, Canada N2L 3G1

ARTICLE INFO

Article history:
Received 22 January 2016
Received in revised form
22 March 2016
Accepted 27 March 2016
Available online 31 March 2016

Keywords:
Three-dimensional ordered macroporous
Li-ion batteries
TiO_2
Flexible
High-power

ABSTRACT

A simple methodology is developed for the in-situ preparation of flexible, three-dimensional ordered macroporous (3DOM) TiO_2 electrodes with greatly enhanced mass transfer. The 3DOM electrode is fabricated using a polystyrene colloidal crystal templated carbon cloth, and provides significant improvements over conventional nanoparticle electrodes without the use of binder or other additive. When evaluated as an anode in a Li-ion battery, the 3DOM electrode provides outstanding high rate performance. The electrode provides a specific capacity of 174 mA h g^{-1} at a current density of 2 A g^{-1}, which is 2.6 times greater than that achieved with a nanoparticle electrode (68 mA h g^{-1}). The 3DOM electrode also achieves excellent cycling stability, with a capacity retention of 94.8% (181 mA h g^{-1}) over 1000 cycles at 10 C (1.7 A g^{-1}) compared to 93.7% (67 mA h g^{-1}) for the nanoparticle electrode. To the best of our knowledge, the performance of our 3DOM electrode is among the highest of binder-free, flexible TiO_2 electrodes. We believe that this methodology is highly useful and is easily transferable to other materials and applications

1. Introduction

Presently, there remains a strong desire to produce flexible energy storage devices that can provide sufficient energy in high-power applications for wearable technologies, automotive vehicles, medical devices, and various flexible consumer products [1,2]. Li-ion batteries (LIBs) are often used for these types of applications because their high energy density [3]. However, their poor charge/discharge rates – specifically when compared to other devices such as supercapacitors – prevents them from providing energy in high-power applications [4]. It is therefore highly desirable to design a flexible energy storage device that can achieve both high energy densities and high power densities. Titanium dioxide (TiO_2) is an anode material in LIBs that shows promise in high-power applications due to its highly reversible lithiation process, lack of solid electrolyte interface (SEI) formation, and relatively small volume expansion [5,6]. TiO_2 is also a highly abundant material, relatively non-toxic, and chemically stable.

Nanoparticle electrodes have been used to address the issue of low power densities in LIBs, which is partially caused by the low solid-state diffusion of Li-ions within the electrode material [7]. However, achieving high-power LIB performance is still a challenge due to nanoparticle aggregation and low mass transfer within the electrode [5]. In a nanoparticle electrode (Fig. 1a), the dense packing of particles reduces overall surface area and surface area contact with the electrolyte. Any uneven distribution of particles and particle sizes will also reduce the uniformity of contact with the electrolyte. Particle sizes must be sufficiently small without aggregation in order to reduce the Li diffusion path and ensure that complete lithiation is kinetically possible. In sufficiently thick electrodes, it is possible that deeper layers of active material will be completely inaccessible for lithiation (highlighted in orange). Electrons in these traditional electrodes are required to overcome interfacial resistance between particles in order to reach the current collector. These interfacial boundaries are marked in the figure by a yellow 'x'. Lastly, nanoparticle electrodes require binding agents and other additives in order to be practical, which can further impede lithiation kinetics and complicate electrode design.

For these reasons, it is necessary to design more functional electrodes that can improve mass transfer and electrode–electrolyte interaction in a battery. An ideal, high-power electrode should have an interconnected structure which allows for efficient mass

* Corresponding authors.
E-mail addresses: aipingyu@uwaterloo.ca (A. Yu), zhwchen@uwaterloo.ca (Z. Chen).

http://dx.doi.org/10.1016/j.nanoen.2016.03.019
2211-2855/

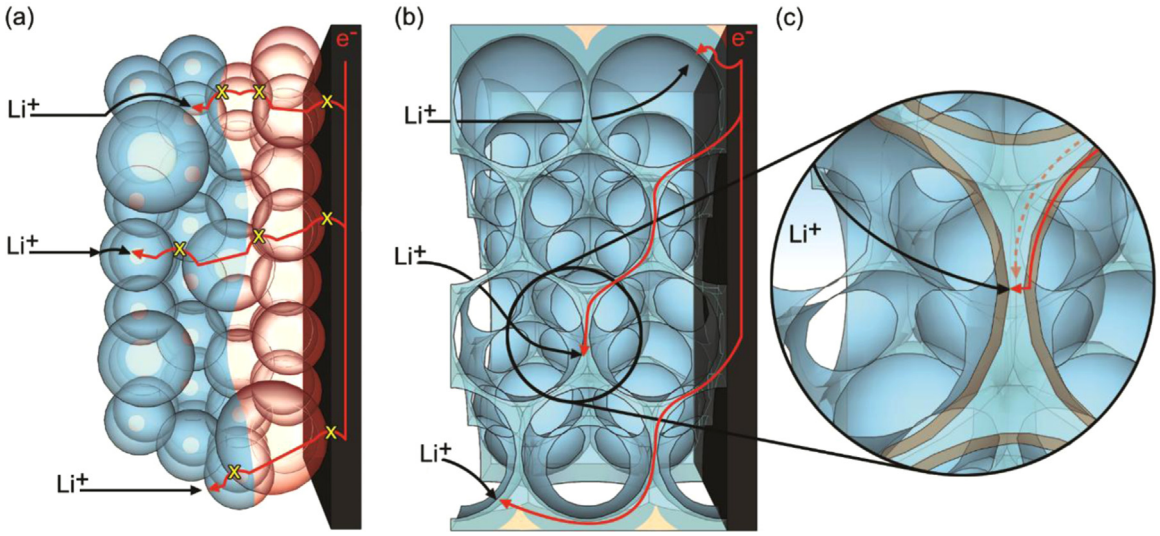

Fig. 1. Diagram comparing lithiation pathways for (a) nanoparticle and (b) 3DOM electrodes. Active material (TiO_2) is blue, potential inaccessible lithiation sites are highlighted in orange, and carbon coating is brown. Interfacial boundaries in the nanoparticle film are marked with a yellow 'x'.

transfer, electron transfer, and contact between the electrode and electrolyte [1,8,9]. Therefore, we have synthesized a flexible, binder-free, three-dimensional ordered macroporous (3DOM) TiO_2 electrode which can provide these characteristics (Fig. 1b). This type of electrode can provide a six-fold advantage compared to nanoparticle electrodes: First, in a 3DOM electrode the ordered porosity of the electrode ensures an even distribution and high surface area contact between the electrode and the electrolyte. This in turn improves mass transfer of ions to the electrode surface and promotes complete lithiation [9,10]. Second, smaller crystallite sizes are easily achieved as they are defined by the colloidal crystal template, and thin pore walls allow for short diffusion paths and complete lithiation at nearly all surface sites [11]. Third, 3DOM structures can allow electron conductivity through its interconnected structure, overcoming interfacial resistances associated with nanoparticle electrodes [12]. Fourth, carbon-coated 3DOM structures (Fig. 1c) can be accomplished in-situ, and can further improve performance by providing alternative, more conductive pathways for electrons. Carbon coating can stabilize the active material during charging and discharging, increasing the cycling stability of the electrode [13]. Fifth, the 3DOM electrode can be easily fabricated using flexible current collectors such as carbon cloth in order to form a flexible electrode. Lastly, the 3DOM electrode can be fabricated without the use of binder or other additive.

This flexible, binder-free 3DOM TiO_2 electrode is achieved by depositing a polystyrene (PS) colloidal crystal template on bare carbon cloth. The PS beads are synthesized using emulsion polymerization and the template is deposited on carbon cloth using a simple dip-coating technique. The templated carbon cloth is then infiltrated with a TiO_2 sol–gel solution and heat-treated to crystallize TiO_2 and remove the template. When calcined in air, the resulting TiO_2 on carbon cloth has a pseudo-3DOM structure. When heat-treated in Ar, the resulting TiO_2 on carbon cloth has a pristine 3DOM structure covered in carbonized polystyrene.

2. Experimental

2.1. Materials

Styrene, polyvinylpyrrolidone (PVP), potassium persulfate, ethanol, hydrochloric acid, and titanium butoxide, and polyvinylidene difluoride were purchased from Sigma Aldrich. Carbon black (Super P) was purchased from MTI. Carbon cloth was purchased from Fuel Cell Earth. All chemicals and materials were used as received.

2.2. 3DOM TiO_2 electrode

Monodisperse polystyrene (PS) beads were synthesized using an emulsion polymerization reaction. First, distilled de-ionized (DDI) water was boiled for several minutes to remove O_2. This water was used for the remainder of the synthesis procedure. 2.5 g polyvinylpyrrolidone surfactant was dissolved in 200 mL DDI water and placed in a three-neck flask. 0.2 g potassium persulfate was dissolved in 40 mL DDI water and placed in a separatory funnel. The PVP solution was brought to 70 °C using an oil bath under stirring. N_2 gas was used to maintain an inert environment. After 10 min, 24 mL styrene monomer was added to the PVP solution and resulting mixture was stirred for 15 min. Lastly, the potassium persulfate solution was added to the monomer solution drop-wise (~1 drop/s) using the separatory funnel. This solution was stirred for 24 h to form the final colloidal PS solution which appears milky white. The concentration of the as-prepared PS solution was adjusted to 30 mg/mL for further use.

Carbon cloth was punched into 12 mm diameter electrodes and cleaned by sonicating in acetone, ethanol, and isopropanol for 20 min each. The carbon cloth electrodes were then dipped in the PS solution and dried at room temperature for several hours to form a PS colloidal crystal template on the surface of the carbon cloth. This process was repeated until a certain mass loading of PS was achieved. This material was denoted as PS-CC.

3DOM TiO_2 on carbon cloth (3T-CC) was obtained by immersing the PS-CC template in a sol–gel solution consisting of 10 mL ethanol, 0.675 mL hydrochloric acid, and 1.415 mL titanium butoxide. The infiltrated electrode was then calcined at 300 °C for 2 h and then 450 °C for 2 h in air using a ramp rate of 1 °C/min in order to burn off the PS template and form anatase TiO_2. 3DOM TiO_2–carbon on carbon cloth (3T-C-CC) was obtained by heat-treating the electrode using the same heating program as for 3T-CC but in Ar to carbonize the PS template.

For comparison, a TiO_2 nanoparticle electrode was synthesized using 25 nm anatase TiO_2 particles. The TiO_2 particles were mixed with carbon black, polyvinylidene difluoride in a ratio of 80:10:10. The slurry was then cast onto a 12 mm diameter carbon cloth electrode and dried at 100 °C in a vacuum oven.

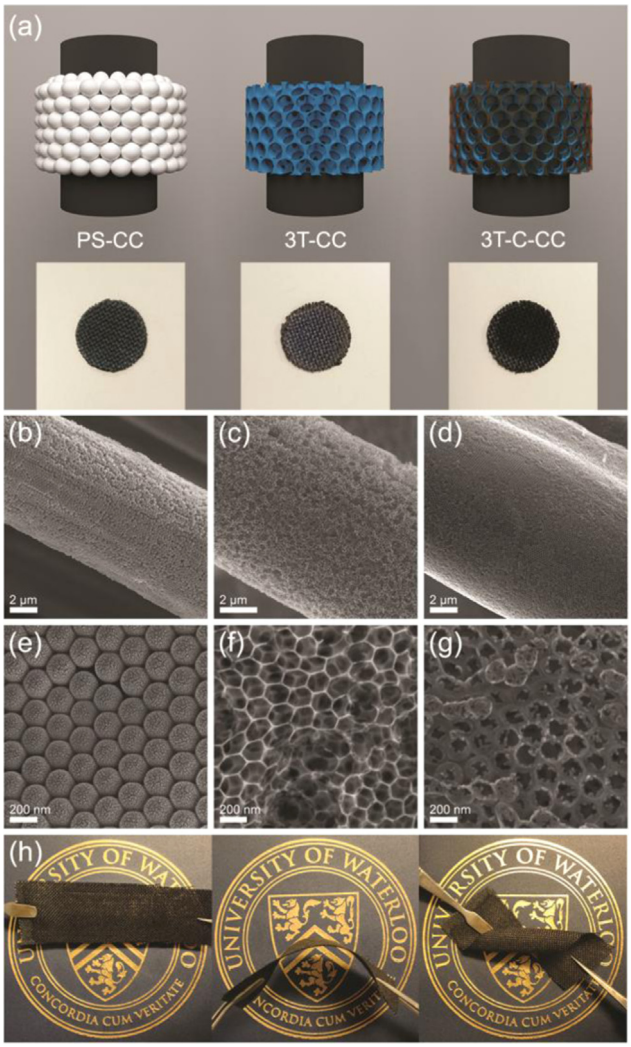

Fig. 2. (a) Schematic drawing of 3T-C-CC synthesis. Low-magnification SEM images of (b) PS-CC, (c) 3T-C, and (d) 3T-C-CC, and high-magnification SEM images of (e) PS-CC, (f) 3T-C, (g) and 3T-C-CC; (g) optical images showing (from left to right) light transmission, bending, and twisting of the as-prepared electrode.

2.3. Characterization

The morphology and microstructure of the synthesized materials were obtained using field-emission scanning electron microscopy (FESEM, Zeiss ULTRA Plus), transmission electron microscopy (TEM, JEOL 2010F), X-ray diffraction (XRD, Rigaku Miniflex600), and Raman spectroscopy (Bruker SENTERRA).

Electrochemical performance of the electrodes in Li-ion batteries was determined by fabricating a 2032 coin-type half-cell. A coin cell was fabricated using Li metal as the counter electrode, a Celgard 2500 separator, and a 7:3 (v/v) ethylene carbonate and dimethyl carbonate electrolyte solution containing 1 M $LiPF_6$. No binder or additive was required for the electrode, and the carbon cloth was used as the current collector. Coin cells were assembled in an Ar-filled glove box with O_2 and H_2O concentrations maintained below 0.5 ppm. Charge–discharge measurements were conducted using a NEWARE BTS-5V10mA battery testing station.

3. Results and discussion

As shown schematically in Fig. 2a, after dipping the carbon cloth in the PS solution, the PS beads self-assemble into a colloidal crystal template along the surface of the carbon cloth fibers (PS-CC). The number of layers of template can be controlled by the number of dip cycles. After infiltrating the PS template with the TiO_2 sol–gel solution and calcining in air, a rough 3DOM TiO_2 film is formed on the carbon cloth fiber (3T-CC). When the templated carbon cloth is heat-treated in Ar, a pristine 3DOM TiO_2 structure covered in carbonized polystyrene is formed on the carbon cloth fibers. This carbonization provides an in-situ, conductive coating for TiO_2. The morphologies of the PS-CC, 3T-CC, and 3T-C-CC electrodes were characterized by scanning electron microscopy (SEM). After the dipping cycles, a continuous layer of PS successfully and uniformly grows on the surface of the carbon fiber with a typical FCC structure (Fig. 2b and e). The PS spheres are monodisperse and approximately 200 nm in diameter. After calcination in air, the 3T-CC electrode can be obtained with thin pore walls and an average pore size of 180 nm which is consistent with the size of PS template (Fig. 2c and f) after a slight reduction in size due to heat treatment [14]. A small portion of broken 3DOM TiO_2 can be observed, which may be attributed to the instability of the colloidal crystal template during heat treatment as well as small imperfections within the template prior to infiltration. By comparison, the 3T-C-CC electrode obtained after heat treatment in Ar is uniformly coated on the carbon fibers (Fig. 2d). The increased wall thickness and decreased pore size (~160 nm) can be found, suggesting successful carbon coating originating from the decomposition and carbonization of the PS (Fig. 2g). Lastly, Fig. 2h shows the stability and flexibility of the as-prepared 3T-C-CC electrode. The carbon cloth maintains its porosity after the deposition of 3DOM TiO_2, allowing light to pass through. The electrodes also retain their form under various forms of mechanical stress – such as bending and twisting – due to the flexibility of the carbon cloth and the strong adhesion of the 3DOM structure to the surface of the carbon cloth. Further testing showed that the electrodes maintained virtually all mass after being subject to severe bending (180°) for 500 cycles (Fig. S4). The strong mechanical stability of the electrode suggests that it can be used in flexible electronic applications.

Fig. 3a and b shows TEM images of the 3T-C structure. The pore size of the 3DOM material is consistent with that found in the SEM images, and the selected area diffraction (SAD) pattern suggests that the material is polycrystalline. The HRTEM image in Fig. 3b clearly shows the amorphous structure of carbon. The image also reveals that the TiO_2 making up the pore walls of the 3DOM material consists of nanocrystalline anatase (d_{101}=0.35 nm) in an amorphous titanium oxide matrix. These anatase crystallites can be seen to be smaller than 5 nm. An EDX map of the 3T-C structure in Fig. 3c shows that Ti, O, and C are present and distributed within the 3DOM structure. The presence and distribution of these elements were further confirmed using SEM energy-dispersive X-ray spectroscopy (EDX) (Fig. S1). An EDX line map was also taken across the pore walls of the 3DOM material (Fig. 3c). The line map clearly shows that Ti and O make up the pore walls, while the pore walls themselves are indeed coated in a carbon layer as shown in the SEM images. This carbon layer can be attributed to the carbonization of polystyrene during the heat treatment process in Ar.

XRD was conducted using Cu Kα radiation (1.54 Å) and is shown in Fig. 3d below. Both 3T-CC and 3T-C-CC electrodes show similar spectra corresponding to anatase TiO_2 (JCPDS no. 21-1272) with characteristic peaks at 2θ=25.6°, 38.1°, 48.3°, 54.1°, 55.0°, and 62.8° [15]. The weak intensity of the anatase peaks is due to the relatively low loading of TiO_2 compared to the carbon cloth. The broad peak centered at approximately 43.7° is due to the presence of carbon cloth while the other characteristic carbon peak at 26.2° is merged with the anatase peak at 25.6° [16]. In order to estimate the true crystallite size of TiO_2, the 3DOM TiO_2 structures were synthesized without carbon cloth. Using the

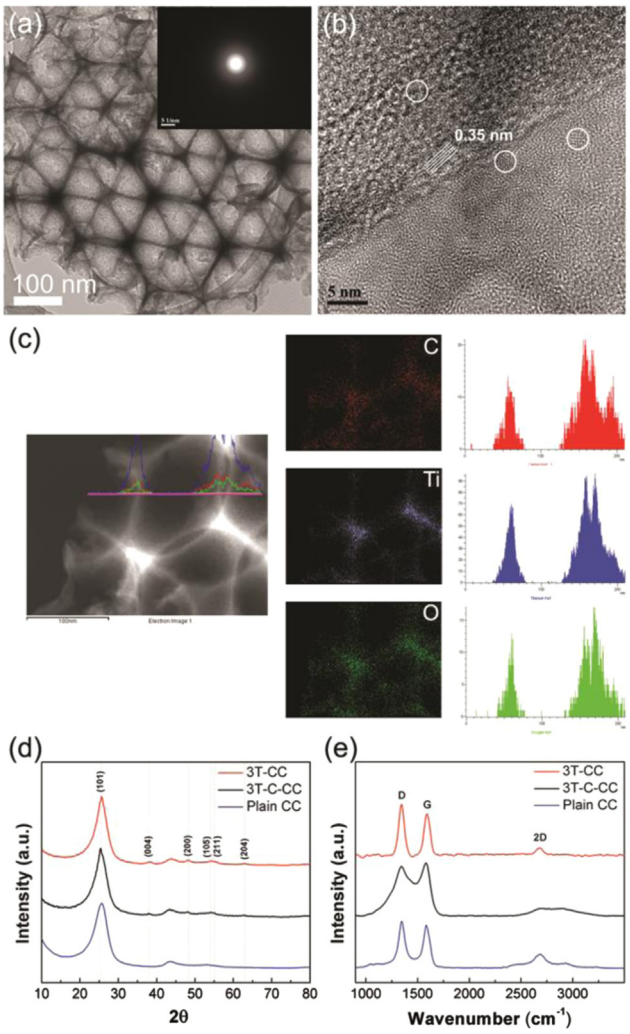

Fig. 3. (a) TEM image of carbon-coated 3DOM structure (inset: corresponding SAED pattern); (b) HRTEM image of pore wall; (c) EDX map and line scan of pore walls showing distribution of C, Ti, and O; (e) XRD and (f) Raman spectra of 3T-CC, 3T-C-CC, and plain carbon cloth.

Scherrer equation, the approximate crystallite size of the 3DOM TiO_2 is 7.6 nm based on the characteristic (101) peak (Fig. S2). This is slightly larger than the crystallite size estimated for the carbon-coated 3DOM TiO_2. It has been shown that crystallite size and particle size match closely at particle sizes lower than 40 nm [17]. It has also been shown that complete lithiation is theoretically possible in crystallites at or below 7 nm. Therefore, the small particle size in the 3DOM TiO_2, along with its highly accessible surfaces can allow for good ion diffusion and lithiation within the macro-structure.

Raman spectroscopy was also used to characterize the graphitic nature of the carbon found in each electrode (Fig. 3e). The spectrum for 3T-CC corresponds to the carbon cloth itself, and finds agreement in literature [18]. In this spectrum, the characteristic D band (1344 cm^{-1}) and G band (1590 cm^{-1}) can be seen, along with a small 2D peak at approximately 2679 cm^{-1} [19]. The spectrum for 3T-C-CC shows a distinct change in the relative intensities of the D and G bands, as well as a broadening of the 2D band. The difference in the Raman spectra has two main consequences. First, the change of D and G band peaks implies that the graphitic nature of the carbon in the electrode has changed due to the addition of carbonized polystyrene. Second, the decrease in the ratio of the D band to the G band (I_D/I_G) implies that the overall degree of disorder in the graphitic structure has decreased with the addition of carbonized polystyrene – confirming that the carbonized polystyrene is amorphous.

The true mass of the TiO_2 active material on the carbon cloth substrate was determined using TGA (Fig. S3). The TGA results show that the mass of the 3T-CC electrode remains constant until approximately 600 °C where the carbon cloth begins to burn away. The TGA curve for 3T-C-CC shows an additional mass change region from 350 °C to 475 °C corresponding to the removal of amorphous carbon from the electrode. In the 3T-C-CC electrode, the amorphous carbon accounts for approximately 3.7% of the total electrode mass. The mass loadings of active material in the 3T-CC and 3T-C-CC electrodes are 6.8% and 6.0%, respectively. This is understandable, as the addition of amorphous carbon in 3T-C-CC will reduce the percent contribution of TiO_2.

The electrochemical behavior of the flexible electrodes was first investigated by cyclic voltammetry using 2032 coin-type half-cells with Li foil as the counter electrode. Fig. 4a shows the representative cyclic voltammetry (CV) curve of 3T-CC and 3T-C-CC flexible electrodes cycled between 3.0 and 1.0 V vs. Li/Li+ at a scan rate of 50 mV s^{-1}. The redox peaks at 2.11 V and 1.69 V correspond to the characteristic lithium insertion and extraction of anatase TiO_2. Two addition redox pairs at 1.55 V/1.48 V and 1.66 V/1.54 V have been reported to correspond to trace amounts of TiO_2-B [20]. However, because no main peaks corresponding to TiO_2-B [21] could be found in the XRD spectra, it is more likely that the peaks correspond to the S-peaks which indicate the presence of amorphous titania in an organized crystalline composite [14,22]. This interpretation is more consistent with the above HRTEM results.

The charge/discharge curves for both 3T-CC and 3T-C-CC at 50 mA h g^{-1} are shown in Fig. 4c below, and show agreement with the obtained CV curve. The plateaus at approximately 1.75 V and 1.9 V correspond to bulk lithiation and de-lithiation processes in TiO_2. It can been seen that the majority of the capacity in both electrodes is dominated by a sloped region which is attributed to a surface-controlled lithium storage process [23]. This understandably corresponds to the highly porous structure of the 3DOM electrode with a highly accessible surface area.

In order to determine the rate performance of the 3T-CC and 3T-C-CC electrodes, each electrode was fabricated into a half-cell and cycled at various charge/discharge rates (Fig. 4b). For comparison, a carbon cloth electrode containing 25 nm anatase particles was fabricated and cycled under the same conditions. Starting at 50 mA h g^{-1}, each electrode is cycled at increasing current densities in order to determine their rate capability. It can be seen that at 50 mA g^{-1}, both 3DOM electrodes have a fairly high initial capacity (401 mA h g^{-1} for 3T-C-CC and 312 mA h g^{-1} for 3T-CC) while the TiO_2 NP electrode has a capacity of 213 mA h g^{-1}. When the current is increased to 2 A g^{-1}, the 3T-CC, 3T-C-CC, and TiO_2 NP electrodes has a stable specific capacities of 115 mA h g^{-1}, 174 mA h g^{-1}, and 68 mA h g^{-1}, respectively. The capacity of the 3T-C-CC electrode finally falls to 69 mA h g^{-1} at a current density of 12.5 A g^{-1}, or ~73.5 C (using $C_{anatase}$ = 170 mA h g^{-1}). The cycling stability of the three electrodes was determined by cycling the electrode at 10 C (1.7 A g^{-1}) for 1000 cycles (Fig. 4d). Based on the discharge capacity of the first and last cycles, the half-cell fabricated using the 3T-C-CC electrode has a capacity retention of 94.8% over 1000 cycles with a final capacity of 181 mA h g^{-1}. Over the same number of cycles, the 3T-CC and TiO2 NP electrodes have a capacity retentions of 79.6% (111 mA h g^{-1}) and 93.7% (67 mA h g^{-1}), respectively. The large difference in stability between 3T-CC and TiO_2 NP-CC is likely due to additives (binder, conductive agent) mixed with the TiO_2 NPs in order to improve its performance. From the cycling results, it is clear that the 3T-C-CC electrode provides the highest cycling stability and highest capacity at 10 C. To the best of our knowledge, this half-cell performance is among the highest found in literature for a flexible, binder-free TiO_2-based electrode [24].

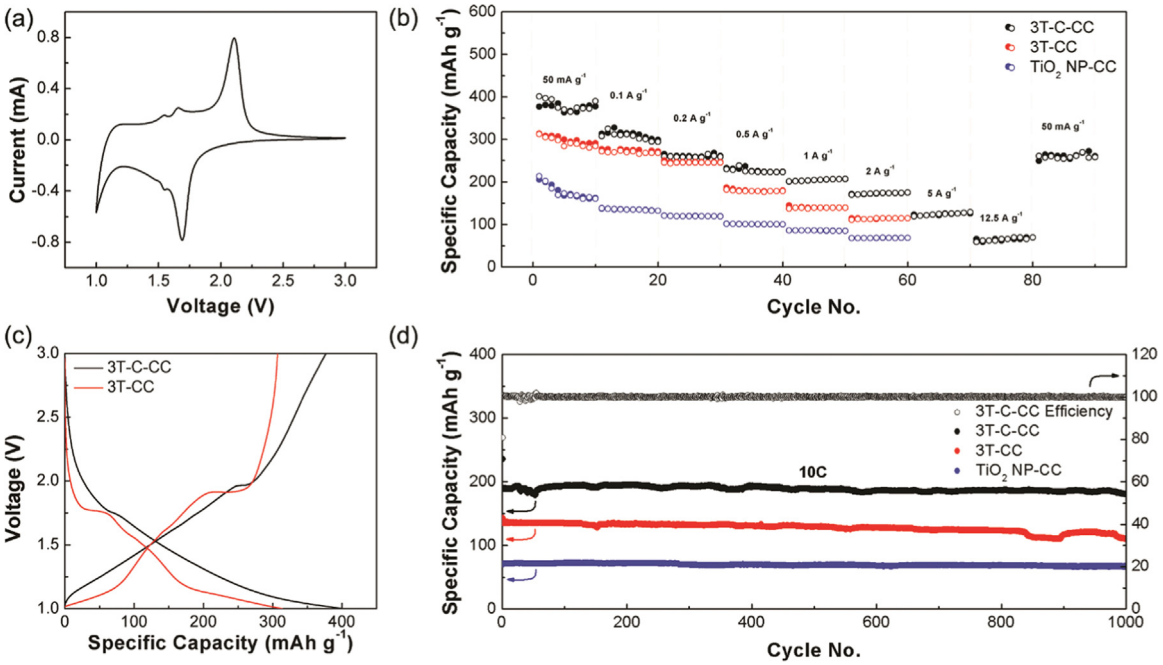

Fig. 4. (a) Representative CV curve of 3DOM TiO_2 material; (b) rate performance of 3T-C-CC, 3T-CC, and TiO_2 NP-CC electrodes; (c) initial charge–discharge curves for 3T-C-CC and 3T-CC electrodes; and, (e) long term cycling of 3T-C-CC, 3T-CC, and TiO_2 NP-CC electrodes at 1.7 A g^{-1} (10 C) for 1000 cycles.

4. Conclusion

In summary, a facile method for synthesizing a flexible, binder-free 3DOM TiO_2 electrode has been shown for the first time. This configuration can act as a flexible, binder-free anode in Li-ion batteries with strong high-power performance. By heat treating the electrode in Ar, the polystyrene template can be used as a source for carbon coating. The resulting carbon-coated 3DOM TiO_2 electrode has superior high-rate performance, with a capacity of 174 mA h g^{-1} at a current density of 2 A g^{-1}. The electrode also shows highly stable performance (181 mA h g^{-1}) with a capacity retention of 94.8% over 1000 cycles at 10 C (1.7 A g^{-1}). This performance is due to the ordered porous structure and thin pore walls of 3DOM TiO_2, which allow for high surface area contact with the electrolyte, and fast lithiation kinetics. This facile method can be easily expanded to other materials and substrates, and can have a vast range of applications in technologies such as supercapacitors, fuel cells, solar cells, and sensors.

Acknowledgements

This work was supported by the Natural Sciences and Engineering Research Council of Canada (NSERC) (Grant no. RGPIN-418319-2012).

Appendix A. Supplementary material

Supplementary data associated with this article can be found in the online version at http://dx.doi.org/10.1016/j.nanoen.2016.03.019.

References

[1] P.G. Bruce, B. Scrosati, J.-M. Tarascon, Angew. Chem. Int. Ed. *47* (2008) 2930.
[2] (a) A. Nathan, A. Ahnood, M.T. Cole, L. Sungsik, Y. Suzuki, P. Hiralal, F. Bonaccorso, T. Hasan, L. Garcia-Gancedo, A. Dyadyusha, S. Haque, P. Andrew, S. Hofmann, J. Moultrie, C. Daping, A.J. Flewitt, A.C. Ferrari, M. J. Kelly, J. Robertson, G. Amaratunga, W.I. Milne, Proc. IEEE 100 (2012) 1486;
(b) H.M. Lee, S.-Y. Choi, A. Jung, S.H. Ko, Angew. Chem. 125 (2013) 7872;
(c) J. Yeo, G. Kim, S. Hong, M.S. Kim, D. Kim, J. Lee, H.B. Lee, J. Kwon, Y.D. Suh, H. W. Kang, H.J. Sung, J.-H. Choi, W.-H. Hong, J.M. Ko, S.-H. Lee, S.-H. Choa, S. H. Ko, J. Power Sources 246 (2014) 562;
(d) S. Lam Po Tang, Trans. Inst. Meas. Control 29 (2007) 283.
[3] (a) F.M. Hassan, R. Batmaz, J. Li, X. Wang, X. Xiao, A. Yu, Z. Chen, Nat. Commun. 6 (2015) 8597;
(b) K. Feng, W. Ahn, G. Lui, H.W. Park, A.G. Kashkooli, G. Jiang, X. Wang, X. Xiao, Z. Chen, Nano Energy 19 (2016) 187.
[4] (a) J.-Y. Liao, X. Xiao, D. Higgins, D. Lee, F. Hassan, Z. Chen, Electrochim. Acta 108 (2013) 104;
(b) J.-Y. Liao, D. Higgins, G. Lui, V. Chabot, X. Xiao, Z. Chen, Nano Lett. *13* (2013) 5467.
[5] G.-N. Zhu, Y.-G. Wang, Y.-Y. Xia, Energy Environ. Sci. *5* (2012) 6652.
[6] H. Liu, W. Li, D. Shen, D. Zhao, G. Wang, J. Am. Chem. Soc. *137* (2015) 13161.
[7] (a) A.K. Rai, L.T. Anh, J. Gim, V. Mathew, J. Kang, B.J. Paul, J. Song, J. Kim, Electrochim. Acta 90 (2013) 112;
(b) S.-T. Myung, M. Kikuchi, C.S. Yoon, H. Yashiro, S.-J. Kim, Y.-K. Sun, B. Scrosati, Energy Environ. Sci. 6 (2013) 2609;
(c) S. Goriparti, E. Miele, M. Prato, A. Scarpellini, S. Marras, S. Monaco, A. Toma, G.C. Messina, A. Alabastri, F.D. Angelis, L. Manna, C. Capiglia, R.P. Zaccaria, ACS Appl. Mater. Interfaces 7 (2015) 25139.
[8] (a) J. Ye, A.C. Baumgaertel, Y.M. Wang, J. Biener, M.M. Biener, ACS Nano 9 (2015) 2194;
(b) M.-J. Deng, C.-Z. Song, P.-J. Ho, C.-C. Wang, J.-M. Chen, K.-T. Lu, Phys. Chem. Chem. Phys. 15 (2013) 7479.
[9] X. Huang, J. Chen, Z. Lu, H. Yu, Q. Yan, H.H. Hng, Sci. Rep. 3 (2013) 2317.
[10] H. Zhang, X. Yu, P.V. Braun, Nat. Nano 6 (2011) 277.
[11] N.S. Ergang, J.C. Lytle, K.T. Lee, S.M. Oh, W.H. Smyrl, A. Stein, Adv. Mater. 18 (2006) 1750.
[12] (a) E.M. Sorensen, S.J. Barry, H.K. Jung, J.R. Rondinelli, J.T. Vaughey, K. R. Poeppelmeier, Chem. Mater. 18 (2006) 1713;
(b) C. Yang, M. Zhou, Q. Xu, Phys. Chem. Chem. Phys. 15 (2013) 19730.
[13] (a) R. Dominko, M. Gaberscek, M. Bele, D. Mihailovic, J. Jamnik, J. Eur. Ceram. Soc. 27 (2007) 909;
(b) S.-J. Park, H. Kim, Y.-J. Kim, H. Lee, Electrochim. Acta 56 (2011) 5355.
[14] L. Kavan, M. Zukalová, M. Kalbáč, M. Graetzel, J. Electrochem. Soc. 151 (2004) A1301.
[15] Y. Xu, E. Memarzadeh Lotfabad, H. Wang, B. Farbod, Z. Xu, A. Kohandehghan, D. Mitlin, Chem. Commun. 49 (2013) 8973.
[16] H. Yu, C. Zhu, K. Zhang, Y. Chen, C. Li, P. Gao, P. Yang, Q. Ouyang, J. Mater. Chem. A 2 (2014) 4551.
[17] M. Wagemaker, W.J.H. Borghols, F.M. Mulder, J. Am. Chem. Soc. 129 (2007) 4323.
[18] N. Padmanathan, S. Selladurai, RSC Adv. 4 (2014) 8341.

[19] A.C. Ferrari, J.C. Meyer, V. Scardaci, C. Casiraghi, M. Lazzeri, F. Mauri, S. Piscanec, D. Jiang, K.S. Novoselov, S. Roth, A.K. Geim, Phys. Rev. Lett. 97 (2006) 187401.
[20] Y. Yang, X. Ji, M. Jing, H. Hou, Y. Zhu, L. Fang, X. Yang, Q. Chen, C.E. Banks, J. Mater. Chem. A 3 (2015) 5648.
[21] L. Wu, D. Bresser, D. Buchholz, S. Passerini, J. Electrochem. Soc. 162 (2015) A3052.
[22] L. Kavan, J. Rathouský, M. Grätzel, V. Shklover, A. Zukal, J. Phys. Chem. B 104 (2000) 12012.
[23] (a) V. Augustyn, P. Simon, B. Dunn, Energy Environ. Sci. 7 (2014) 1597;
(b) Z. Chen, D. Zhang, X. Wang, X. Jia, F. Wei, H. Li, Y. Lu, Adv. Mater. 24 (2012) 2030.
[24] (a) J. Cheng, B. Wang, H.L. Xin, C. Kim, F. Nie, X. Li, G. Yang, H. Huang, J. Mater. Chem. A 2 (2014) 2701;
(b) T. Hu, X. Sun, H. Sun, M. Yu, F. Lu, C. Liu, J. Lian, Carbon 51 (2013) 322;
(c) S. Liu, Z. Wang, C. Yu, H.B. Wu, G. Wang, Q. Dong, J. Qiu, A. Eychmüller, X. W. Lou, Adv. Mater. 25 (2013) 3462;
(d) S. Lee, J. Ha, J. Choi, T. Song, J.W. Lee, U. Paik, ACS Appl. Mater. Interfaces 5 (2013) 11525.

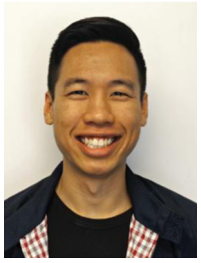

Gregory Lui received his master's degree in Chemical Engineering in 2014 from the University of Waterloo, Canada, and is currently continuing his studies as a Ph. D. Candidate in Chemical Engineering (Nanotechnology) at the same institution. His current research interests involve the design and synthesis of nanomaterials in various clean energy and energy storage systems, including photocatalysts, photoelectrochemical devices, and li-ion batteries.

Dr. Ge Li obtained her Ph.D. in 2012 from East China Normal University, P.R. China. She was a visiting student at the University of California, Los Angles from 2010 to 2012. She joined the University of Waterloo as a postdoctoral researcher in 2014. Currently, she is working on the development of advanced composite materials for supercapacitors, lithium-sulfur batteries, and electrocatalysts.

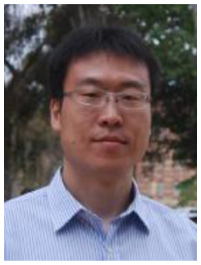

Dr. Xiaolei Wang received his master's degree from Tianjin University in 2007, and then obtained his Ph.D. in Chemical Engineering from the University of California, Los Angeles in 2013. Currently, he is a postdoctoral researcher at the University of Waterloo, Canada. His research interest mainly focuses on the design and development of advanced materials for energy storage applications.

Gaopeng Jiang received his master's degree from Donghua University in 2012 and is currently a Ph.D. candidate in Chemical Engineering (Nanotechnology) at the University of Waterloo, Canada. His research interest mainly focuses on the design and development of nanostructured materials for energy storage and conversion devices including fuel cells, batteries, and sensors.

Edric Lin is currently an undergraduate student who began studying Chemical Engineering at the University of Waterloo, Canada, in 2014. His research interests include biomimicry and the production of commercially viable bio-inspired adhesives and hydrophobic materials.

Dr. Michael Fowler is a Professor in the Department of Chemical Engineering at the University of Waterloo with a research interest in electrochemical power sources. Specifically his research focuses on fuel cell system design and reliability, fuel cell and battery materials durability, and green power systems. His research includes modelling of hydrogen production and distribution systems, including Power-to-Gas. With the University of Waterloo Alternative Fuels team he is the co-advisor of the development of a number of fuel cell and plug-in hybrid vehicles. The University of Waterloo is one of Canada's leading comprehensive universities with extensive graduate and undergraduate programs.

Dr. Aiping Yu is an Associate Professor at University of Waterloo. Her research interests are materials development for supercapacitors, photocatalysts and nanocomposites. She has published over 65 papers in peer-reviewed journals, 3 book chapters, and one book. These publications have received more than 6300 citations. Her work has been featured by major media reports such as Nature Nanotechnology, Wall Street News, Photonics.com, and Azonano.com. She has held 7 patents and provisional patents, and 2 of her patents have been licensed to industry. She is also an editorial board member of Scientific Report, nature publishing group.

Dr. Zhongwei Chen is a Canada Research Chair Professor in Advanced Materials for Clean Energy at University of Waterloo. His research interests are in the development of advanced energy materials for metal-air batteries, lithium-ion batteries, and fuel cells. He has published 1 book, 7 book chapters, and more than 150 peer reviewed journal articles with over 10,000 citations (H-index=44). He is listed as an inventor on 15 US/international patents, with several licensed to companies in North America. He is the recipient of various awards, including the 2016 E.W.R Steacie Memorial Fellowship, Ontario Early Researcher Award, NSERC Discovery Supplement Award, and Distinguished Performance and Research Excellence Awards from the University of Waterloo.